Available online at www.elixirpublishers.com (Elixir International Journal)

Vibrational Spectroscopy

Elixir Vib. Spec. 71A (2014) 25178-25187

ISSN: 2229-712X

FT-IR and Raman Spectra Vibrational Assignments and Density Functional Calculations of 2-methoxynaphthalene

G.Venkatesh[1,*], M.Govindaraju[2] and P.Vennila[3]

[1]Research and Development Centre, Bharathiar University, Coimbatore - 641 046, India.

[2]Department of Chemistry, Kongu Polytechnic College, Erode- 638052, India.

[3]Department of Chemistry, Thiruvalluvar Govt. Arts College, Rasipuram, Tamilnadu, India.

ARTICLE INFO

Article history:

Received: 20 April 2014;

Received in revised form:

2 June 2014;

Accepted: 15 June 2014;

Keywords

Density Functional Theory,
FT-Raman, FT-IR,
HOMO, LUMO, NBO,
First-order Hyperpolarizability,
Electronic Excitation Energy.

ABSTRACT

The Fourier transform Infrared (FT-IR) and FT-Raman spectra of 2-Methoxynaphthalene (2MN) have been measured. The molecular geometry, vibrational frequencies, Infrared intensities and Raman activities have been calculated by using density functional theory calculation (B3LYP) with 6-311+G** basis set. Complete vibrational assignment and analysis of the fundamental modes of the compound were carried out using the observed FT-IR and FT-Raman. Simulated FT-IR and FT-Raman spectra for 2MN showed good agreement with the observed spectra. The stability of the molecule arising from hyper conjugative interactions and the charge delocalization has been analyzed using natural bond (NBO) analysis. Further, density functional theory (DFT) combined with quantum chemical calculations to determine the first-order hyperpolarizability. The calculated HOMO and LUMO energies show that charge transfer occurs within the molecule. Electronic excitation energies, oscillator strength and nature of the respective excited states were calculated by the closed-shell singlet calculation method were also calculated for the molecule.

Introduction

Vibrational spectroscopy is used extensively in organic chemistry, for the identification of functional groups of organic compounds, for studies on molecular conformation, reaction kinetics, etc [1]. Due to the great biochemical importance the vibrational spectral studies of 2-Methoxynaphthalene (2MN) have been carried out in the present investigation. Naphthalene and its derivatives are biologically, pharmaceutically and industrially useful compounds. The structure of naphthalene is benzene-like, having two–six membered rings fused together. Particularly, naphthalene was studied because, of its technological applications in a vast amount of industrial process. In fact, it was used as a precursor for the synthesis of plastics and dyes, gamma-ray detector in photo multiplier tubes and also used in dye stuffs, synthetic resins, coatings, tanning agent and celluloid [2]. Though the lower acids like formic and cetic acids have been extensively studied and few studies exist for the higher acids.

Modern vibrational spectrometry has proven to be an exceptionally powerful technique for solving many chemical problems. It has been extensively employed both in the study of chemical kinetics and chemical analysis. The problem of signal assignment however, as well as understanding the relationship between the observed spectral features and molecular structure, and reactivity can be difficult. Even identification of fundamental vibrational frequencies often generates controversy. FT-IR, FT-Raman spectroscopy combined with quantum chemical computations has been recently used as an effective tool in the vibrational analysis of drug molecules [3], biological compounds [4] and natural products, since fluorescence-free Raman spectra and the computed results can help unambiguous identification of vibrational modes as well as the bonding and structural features of complex organic molecular systems. The present work deals with density functional theoretical (DFT) computations and vibrational spectral analysis of 2-methoxynaphthalene [2MN]. The geometrical parameters of the most optimized geometry obtained via energy calculations were used for the DFT calculations. The Infrared and Raman intensities were also predicted, based on these calculations, the simulated FTIR and FT-Raman spectra were obtained. The observed and the simulated spectra agree well.

Experimental Details

The compound 2MN was purchased from the Sigma–Aldrich Chemical Company (USA) with a stated purity of greater than 98% and it was used as such without further purification. The FT-Raman spectra of 2MN was recorded using 1064 nm line of Nd:YAG laser as excitation wavelength in the region 4000–100 cm^{-1} on a Brucker model IFS 66 V spectrophotometer equipped with FRA 106 FT-Raman module accessory. The room temperature FT-IR spectrum of this compound was recorded in the region 4000-400 cm^{-1} on IFS 66V spectrophotometer using KBr pellet technique.

Computational Details

The entire calculations were performed at B3LYP levels using GAUSSIAN 09W [5] program package, invoking gradient geometry optimization [6]. Initial geometry generated from standard geometrical parameters was minimized without any constraint in the potential energy surface at DFT level adopting the standard B3LYP/6-311+G** basis set. The optimized structural parameters were used in the vibrational frequency calculations at the DFT levels to characterize all stationary points. Then vibrationally averaged nuclear positions of 2MN were used for harmonic vibrational frequency calculations resulting in IR and Raman frequencies together with intensities and Raman depolarization ratios. We have utilised the gradient corrected density functional theory (DFT) [7] with the three-

Tele: +91-9965285541

E-mail addresses: venkateshindhuja@gmail.com

parameter hybrid functional (B3) [8] for the exchange part and the Lee–Yang–Parr (LYP) correlation function [9], accepted as a cost-effective approach, for the computation of molecular structure, vibrational frequencies and energies of optimized structures. Vibrational frequencies computed at DFT level have been adjudicated to be more reliable than those obtained by the computationally demanding Moller–Plesset perturbation methods. Finally, the calculated normal mode vibrational frequencies provide thermodynamic properties also through the principle of statistical mechanics.

By combining the results of the GAUSSVIEW program [10] with symmetry considerations, vibrational frequency assignments were made with a high degree of accuracy. There is always some ambiguity in defining internal coordination. However, the defined coordinate form complete set and matches quite well with the motions observed using the GAUSSVIEW program.

The Raman activities (Si) calculated with the GAUSSIAN 09W program and adjusted during the scaling procedure with MOLVIB were subsequently converted to relative Raman intensities (Ii) using the following relationship derived from the basic theory of Raman scattering [11-12].

$$I_i = \frac{f(v_o - v_i)^4 S_i}{v_i[1-\exp(-hcv_i / KT)} \text{ ----------(1)}$$

Where υ_0 is the exciting frequency (in cm^{-1}), υ_i is the vibrational wavenumber of the i^{th} normal mode; h, c and k are fundamental constants, and f is a suitably chosen common normalization factor for all peak intensities.

Results and discussion

Molecular geometry

The molecular structure of 2MN is shown in Fig 1. The global minimum energy obtained by the DFT structure optimization for the title compound is presented in Table 1. The bond lengths and bond angles determined at the DFT level of theory for the 2MN compound are listed in Table 2.

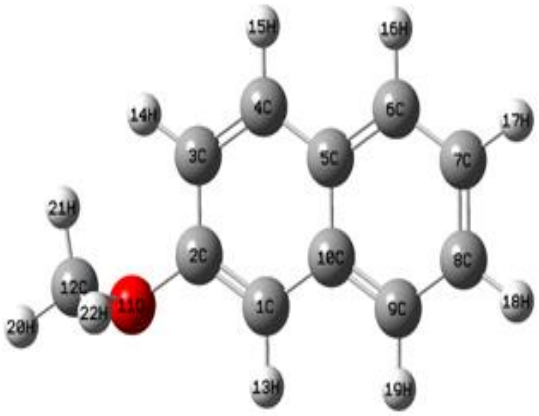

Fig 1. The optimized molecular structure of 2MN

Table 1. Total energies of 2MN, calculated at DFT B3LYP/6-31G* and B3LYP/6-311+G level**

Method	Energies (Hartrees)
6-31G*	-500.32544894
6-311+G**	-500.41414352

The geometrical optimization studies of 2MN reveal that the molecule belongs to C_s symmetry point group. Detailed descriptions of vibrational modes can be given by means of normal coordinate analysis. For this purpose, the full set of 81 standard internal coordinates containing 21 redundancies for 2MN was defined as given in Table 3. From there non redundant set of local symmetry coordinates was constructed by suitable liner combinations of internal coordinates following the recommendations of Fogarasi and Pulay [13-15] is presented in Table 4. The theoretically calculated DFT force fields were transformed in this later set of vibrational coordinates and used in all subsequent calculations.

Vibrational assignments

The vibrational assignments in the present study are based on the scaled DFT/6-311+G** frequencies, Infrared intensities, Raman activities, as well as characteristic "group frequencies" from similar molecules. The 60 normal modes of 2MN are distributed among the symmetry species as Γ_{3N-6}= 41 A' (in-plane) + 19 A″ (out-of-plane), and in agreement with C_s symmetry. All the vibrations were active both in Raman scattering and Infrared absorption.

The detailed vibrational assignments of fundamental modes of 2MN along with the observed and calculated frequencies, IR and Raman intensities and normal mode descriptions are depicted in Table 5. For visual comparison, the observed and simulated FT-IR and FT-Raman spectra of 2MN are produced in a common frequency scales in Fig 2 & Fig 3.

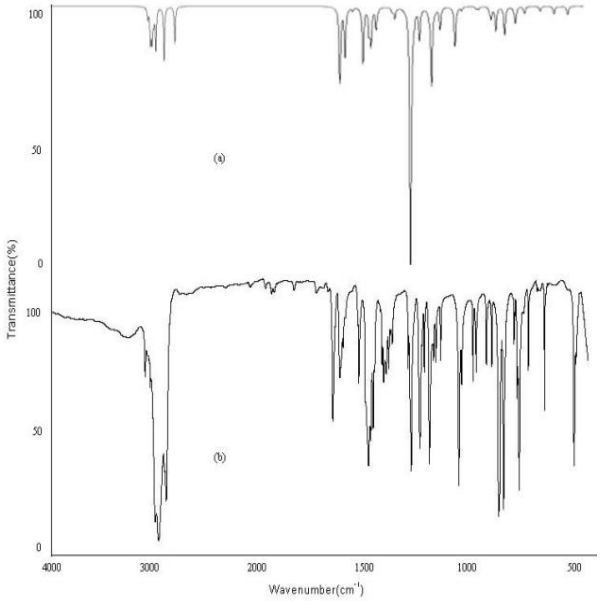

Fig 2. FT-IR spectra of 2MN (a)Calculated (b) Observed with B3LYP/6-311+G**

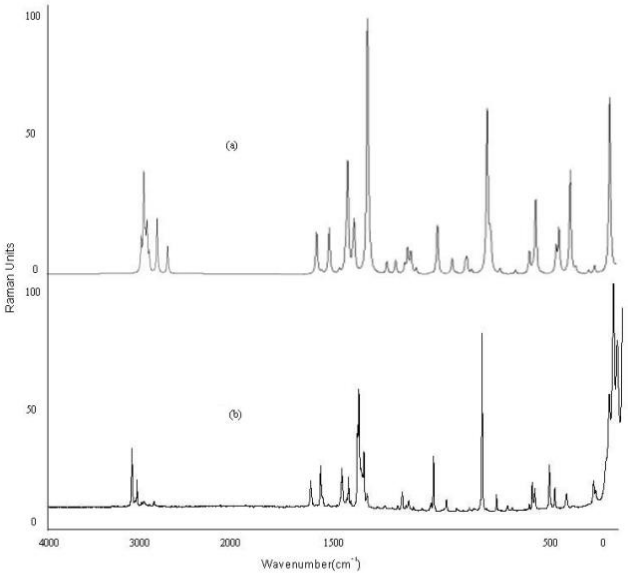

Fig 3. FT-Raman spectra of 2MN
(a) Calculated (b) Observed with B3LYP/6-311+G**

Root mean square (RMS) values of frequencies were obtained in the study using the following expression,

$$RMS = \sqrt{\frac{1}{n-1}\sum_{i}^{n}\left(\upsilon_i^{calc} - \upsilon_i^{exp}\right)^2}$$

The RMS error of frequencies (B3LYP/6-311+G**) obtained for 2MN was found to be 113 cm^{-1}. In order to reproduce the observed frequencies, refinement of scaling factors was applied and optimized via least square refinement algorithm which resulted a RMS deviation of 7.45 cm^{-1}. The good agreement allows us to perform the assignments of the IR and Raman bands to the normal modes in the whole studied spectral regions. From high to low wave number the following comments are in order.

C-H vibrations

The characteristic C-H stretching vibrations of heteromatic structure is expected to appear in 3300-3100 cm^{-1} frequency ranges [16]. The theoretical vibrations assigned to 3185, 3184, 3159 and 3191, 3161, 3158 cm^{-1} in FT-IR and FT-Raman spectrum respectively. The recorded FT-IR spectrum show the bands at 3018, 3016 and 3014 cm^{-1}. The bands due to C-H in-plane ring bending vibrations, interacting with C-C stretching vibrations, are observed as a number of medium-strong intensity sharp bands in the region 1300-1000 cm^{-1}. The C-H out-of-plane bending vibrations are strongly coupled vibrations occur in the region 950-750 cm^{-1}. The frequencies 1320-1190 cm^{-1} are assigned to C-H in-plane-bending vibrations are in good agreement with values given in literature [17] and also recorded FT-IR gas phase spectral values at 1320, 1318, 1316, 1224, 1221 cm^{-1} and 1273, 1272, 1269, 1197, 1196, 1192 cm^{-1} in FT-Raman spectral values are assigned to C-H in-plane-bending vibration. The recorded values at 1050, 1049, 1047, 824, 822, 819 cm^{-1} in FT-IR spectrum and 992, 990, 962, 961, 897, 891 cm^{-1} in FT-Raman spectrum are assigned to C-H out-of plane bending vibration.

C-C vibrations

Naphthalene ring stretching vibrations are expected in the region 1620-1390 cm^{-1}. Naphthalene ring vibrations are found to make a major contribution in the IR and Raman spectra [18,19], the frequency observed in the FT-IR spectrum as a medium and strong bands at 1623, 1622, 1502, 1499, 1419, 1418 and 1414 cm^{-1} have been assigned to C-C stretching vibrations. The same vibrations appear in the FT-Raman spectrum at 1667, 1665, 1571, 1570, 1568, 1495, 1493, 1490 and 1404 cm^{-1}. The theoretically predicated values at 1611-1338 cm^{-1} and at 1596-1339 cm^{-1} respectively show excellent agreement with experimental data. These vibrations are mixed up with C-H in-plane-bending vibrations as shown in Table 5. The in-plane deformation vibration is at higher frequencies than that out-of-plane vibrations. Shimanouchi et al. [20] gave the frequency data for these vibrations for different derivatives as a result of normal coordinate analysis. The bands observed at 1050, 1049 and 1047 cm^{-1} in FT-IR spectrum and 1165, 1163 and 1161 cm^{-1} in FT-Raman spectrum are assigned to C-C in plane bending vibrations [21-23]. The C-C-C out-of-plane deformation computed method also show good agreement with recorded spectral data.

C–O vibrations

The C-O stretching vibration is expected in the region 1330-1430 cm^{-1}. The C-O bond formed by Рл-Рл between C and O intermolecular hydrogen bonding reduces the frequencies of the C-O stretching absorption to a greater degree than does intermolecular H bonding because of the different electro-negativities of C and O, the bonding are not equally distributed between the two atoms[24]. In our present study a very strong band observed in FT-IR spectrum at 1320, 1318 and 1316 cm^{-1} is assigned to C-O stretching vibrations show good agreement. The recorded FT-Raman has very strong band at 1404 cm^{-1} is assigned to C-O stretching vibration.

Ring vibrations

In the preset study, the bands observed at 1320, 1318 and 1316 cm^{-1} and 1273, 1272 and 1269 cm^{-1} in FT-IR and FT-Raman, respectively are attributed to ring in-plane bending modes. The ring out-of-plane bending mode frequencies are established at 824, 822, 819, 636, 635 and 632 cm^{-1} in IR and 897, 896 and 891 cm^{-1} in Raman spectra as shown in Table 5.

Methyl group vibrations

For the assignments of CH_3 group frequencies, one can expect that nine fundamentals can be associated to each CH_3 group, namely the symmetrical (CH_3 ips) and asymmetrical (CH_3 ops), inplane stretching modes (i.e. in-plane hydrogen stretching mode); the symmetrical (CH_3 ss), and asymmetrical (CH_3 ips), deformation modes; the in-plane rocking (CH_3 ipr) out-of-plane rocking (CH_3 opr) and twisting (t CH_3) bending modes.

In addition to that, the asymmetric stretching (CH_3 ops) and asymmetric deformation (CH_3 opb) modes of the CH_3 group are expected to be depolarised for A'' symmetry species. The CH_3 ss stretching vibrations are observed at 3018, 3016 and 3014 cm^{-1} in FT-IR frequencies. The Infrared band observed at 3159, 3161 and 3018 cm^{-1} in CH_3 ips and CH_3 ops stretching vibrations. In accordance with the CH_3 sb and CH_3 ipb vibrations in 2MN has been identified at 1542, 1540, 1536 cm^{-1} and 1529, 1528 and 1524 cm^{-1} by B3LYP/6-311+G** method. The theoretically calculated CH_3 out-of-plane and in-plane bending modes have been found to be consistant with the recorded spectral values [25,26].

NBO analysis

Natural bond analysis is an accurate possible natural Lewis structure picture because all orbital mathematically chosen to include the highest possible percentage of the electron density. Interaction between both filled and virtual orbital spaces information correctly explained by the NBO analysis, it could enhance the analysis of intra- and intermolecular interactions. The second order Fock matrix was carried out to evaluate donor (i) acceptor (j) i.e. donor level bonds to acceptor level bonds interaction in the NBO analysis [27]. The result of interaction is a loss of occupancy from the concentrations of electron NBO of the idealized Lewis structure into an empty non-Lewis orbital. For each donor (i) and acceptor (j), the stabilization energy E(2) associates with the delocalization, i to j is estimated as:

$$E(2) = \Delta E_{ij} = n_i\left[\frac{F(i,j)^2}{\left(\varepsilon_j - \varepsilon_i\right)}\right]$$

where q_i is the donor orbital occupancy, areδ_j and δ_i diagonal elements and F(i, j) is the off diagonal NBO Fock matrix element. Natural bond orbital analysis is used for investigating charge transfer or conjugative interaction in the molecular system. Some electron donor orbital, acceptor orbital and the interacting stabilization energy resulted from the second-order micro-disturbance theory are reported [28,29]. The larger E(2), value the more intensive is the interaction between electron donors and acceptor, i.e. the more donation tendency from electron donors to electron acceptors and the greater the extent of conjugation of the whole system [30].

Table 2. Optimized geometrical parameters of 2MN obtained by B3LYP/6–311+G density functional calculations**

Bond length	Value(Å)	Bond angle	Value(Å)	Dihedral angle	Value(Å)
C2-C1	1.38599	C3-C2-C1	119.59676	C4-C3-C2-C1	-0.69212
C3-C2	1.38603	C4-C3-C2	119.59886	C5-C4-C3-C2	0.46301
C4-C3	1.38599	C5-C4-C3	119.99631	C6-C5-C4-C3	179.42720
C5-C4	1.38599	C6-C5-C4	119.99771	C7-C6-C5-C4	-179.42716
C6-C5	1.38604	C7-C6-C5	119.99894	C8-C7-C6-C5	-1.82760
C7-C6	1.38600	C8-C7-C6	122.91708	C9-C8-C7-C6	2.73878
C8-C7	1.38642	C9-C8-C7	113.89579	C10-C1-C2-C3	0.45822
C9-C8	1.38600	C10-C1-C2	120.00100	O11-C2-C1-C10	-178.96691
C10-C1	1.38599	O11-C2-C1	119.99966	C12-O11-C2-C1	119.99554
O11-C2	1.40998	C12-O11-C2	120.01944	H13-C1-C2-C3	-178.95914
C12-O11	1.41001	H13-C1-C2	120.02202	H14-C3-C2-C1	179.88290
H13-C1	1.12204	H14-C3-C2	119.99838	H15-C4-C3-C2	-178.96503
H14-C3	1.12201	H15-C4-C3	116.98241	H16-C-C5-C4	1.14480
H15-C4	1.12204	H16-C-C5	123.05333	H17-C7-C6-C5	178.74458
H16-C6	1.12194	H17-C7-C6	119.99346	H18-C8-C7-C6	-176.68454
H17-C7	1.12202	H18-C8-C7	120.00472	H19-C9-C8-C7	178.74455
H18-C8	1.12201	H19-C9-C8	119.99656	H20-C12-O11-C2	-180.00000
H19-C9	1.12194	H20-C12-O11	109.49454	H21-C12-O11-C2	59.93269
H20-C12	1.12198	H21-C12-O11	109.49887	H22-C12-O11-C2	-59.92966
H21-C12	1.12199	H22-C12-O11	109.50320		
H22-C12	1.12193				

*for numbering of atom refer Fig 1

Table 3. Definition of internal coordinates of 2MN

No(i)	symbol	Type	Definition
Stretching 1-11	r_i	C-C	C1-C2,C2-C3,C3-C4,C4-C5,C5-C6, C6-C7,C7-C8,C8-C9,C9-C10,C10-C5,C10-C1
12-18	S_i	C-H	C1-H13,C3-H14,C4-H15,C6-H16, C7-H17,C8-H18,C9-H19
19-20	p_i	C-O	C2-O11,C12-O11.
21-23	P_i	C-H(m)	C12-H20,C12-H21,C12-H22
Bending 24-29	α_i	C-C-C	C1-C2-C3,C2-C3-C4,C3-C4-C5, C4-C5-C10,C5-C10-C1,C10-C1-C2
30-35	n_i	C-C-C	C6-C7-C8,C7-C8-C9,C8-C9-C10, C9-C10-C5,C10-C5-C6,C5-C6-C7
36-49	θ_i	C-C-H	C2-C1-H13,C10-C1-H13,C2-C3-H14,C4-C3-H14,C3-C4-H15,C5-C4-H15,C5-C6-H16,C7-C6-H16,C6-C7-H17,C8-C7-H17,C7-C8-H18,C9-C8-H18,C8-C9-H19,C10-C9-H19
50-51	β_i	C-C-O	C3-C2-O11, C1-C2-O11
52	Φ_i	C-O-C	C2-O11-C12
53-55	μ_i	H-C-H	H20-C12-H21,H21-C12-H22,H22-C12-H20
56-58	ν_i	O-C-H	O11-C12-H20,O11-C12-H21,O11-C12-H22
Out-of-plane 59-65	ω_i	C-H	H13-C1-C2-C10,H14-C3-C2-C4,H15-C4-C3-C5,H16-C6-C5-C7,H17-C7-C6-C8, H18-C8-C9-C7,H19-C9-C8-C10.
66	ξ_i	C-O	O11-C2-C1-C3
Torsion 67-72	τ_i	τC-C	C1-C2-C3-C4,C2-C3-C4-C5,C3-C4-C5-C10,C4-C5-C10-C1,C5-C10-C1-C2,C10-C1-C2-C3
73-78	τ_i	τC-C	C6-C7-C8-C9,C7-C8-C9-C10,C8-C9-C10-C5,C9-C10-C5-C6,C10-C5-C6-C7,C5-C6-C7-C8
79	τ_i	τC-O	C1(C3)-C2-O11-C12
80	τ_i	τC-H	C2-O11-C12-(H20,H21,H22)
81	τ_i	τbutter	C4(C6)-C5-C10-C9(C1)

*for numbering of atom refer Fig 1

Table 4. Definition of local symmetry coordinates and the value corresponding scale factors used to correct the force fields for 2MN

No.(i)	Symbol[a]	Definition[b]	Scale factors used in calculation
1-11	C-C	r1,r2,r3,r4,r5,r6,r7,r8,r9,r10,r11	0.914
12-17	C-H	S12,S13,S14,S15,S16,S17,S18	0.914
18-19	C-O	p18,p19	0.992
20-23	C-H(m)	P20,P21,P22,P23	0.992
24	bring1	(α24-α25+α26-α27+α28-α29)/ √6	0.992
25	bring1	(2α24-α25-α26+2α27-α28-α29)/ √12	0.992
26	bring1	(α25-α26+α28-α29)/2	0.992
27	bring2	(n30-n31+n32-n33+n34-n35)/ √6	0.992
28	bring2	(2n30-n31-n32+2n33-n34-n35)/ √12	0.992
29	bring2	(n31-n32+n34-n35)/2	0.992
30-36	C-C-H	(θ36-θ37)/√2,(θ38-θ39)/√2,(θ40-θ41)/√2,(θ42-θ43)/√2,(θ44-θ45)/√2,(θ46-θ47)/√2,(θ48-θ49)/√2	0.916
37	C-C-O	(β50-β51)/√2	0.923
38	C-O-C	Φ52	0.923
39	msb	(μ53+μ54+μ55-ν56-ν57-ν58)/ √6	0.923
40	mipb	(2μ55-μ53-μ54)/ √6	0.923
41	mopb	(μ53-μ55)/ √2	0.923
42	mipr	(2ν57-ν56-ν58)/ √6	0.923
43	mopr	(ν59-ν58)/ √2	0.923
44-50	C-H	ω59, ω60, ω61, ω62, ω63, ω64, ω65	0.994
51	C-O	ξ66	0.962
52	tring1	(τ67-τ68+τ69-τ70+τ71-τ72)/√6	0.994
53	tring1	(τ68-τ69+τ70-τ72)/2	0.994
54	tring1	(-τ67+2τ68-τ69-τ70+2τ71-τ72)/√12	0.994
55	tring2	(τ73-τ74+τ75-τ76+τ77-τ78)/√6	0.994
56	tring2	(τ74-τ75+τ76-τ78)/2	0.994
57	tring2	(-τ73+2τ74-τ75-τ76+2τ77-τ78)/√12	0.994
58	C-O	τ79	0.979
59	N-O	τ80/3	0.979
60	butter	τ81	0.979

[a] These symbols are used for description of the normal modes by TED in Table 5.
[b] The internal coordinates used here are defined in Table 3.

Table 5. Detailed assignments of fundamental vibrations of 2MN by normal mode analysis based on SQM force field calculation

S. No.	Symmetry species C_s	Observed frequency (cm^{-1})		Calculated frequency (cm^{-1}) with B3LYP/6-311+G ** force field				TED (%) among type of internal coordinates[c]
		Infrared	Raman	Unscaled	Scaled	IR[a] A_i	Raman[b] I_i	
1	A'	3231		3230	3228	13.505	124.677	CH(99)
2	A'		3213	3212	3209	29.247	340.756	CH(99)
3	A'	3210		3209	3205	13.339	63.864	CH(99)
4	A'			3198	3195	34.206	93.342	CH(99)
5	A'		3191	3189	3184	11.744	140.108	CH(99)
6	A'	3184		3185	3181	2.074	41.722	CH(99)
7	A'			3182	3177	2.799	8.766	CH(99)
8	A'	3159	3161	3160	3158	45.918	66.221	mips(75),mops(24)
9	A'			3097	3094	58.652	197.625	mops(55),mss(25),mips(19)
10	A'	3018		3016	3014	40.159	91.660	mops(63),mips(21),mss(15)
11	A'			1692	1690	82.494	36.600	CC(66),bCCH(16),bring1(9),bring2(7)
12	A'		1667	1665	1662	53.369	2.317	CC(66),bCCH(23)
13	A'	1623		1625	1622	3.379	37.428	CC(72),bCCH(13),bring2(7),bring1(6)
14	A'		1571	1570	1568	61.757	2.895	CC(53),bCCH(36)
15	A'	1542		1540	1536	25.532	11.036	bmipb(76),bmopr(7)
16	A'			1531	1526	35.416	54.075	bCCH(40),CC(28),bmsb(13),bmipb(7),CO(6)
17	A'		1528	1529	1524	5.171	31.695	bmopb(56),bmipb(43)
18	A'	1502		1501	1499	23.187	6.753	bmsb(73),bCCH(16),CC(8)
19	A'		1495	1493	1490	3.209	34.446	bCCH(45),CC(43)
20	A'			1422	1419	0.038	154.372	CC(84),bCCH(11)
21	A'	1419		1418	1414	4.776	17.393	CC(57),bCCH(37)
22	A'		1404	1406	1400	13.486	4.275	CC(58),bCCH(29),bCO(5)
23	A'	1320		1318	1316	286.290	6.724	CO(42),bCCH(18),CC(17),bring1(10)
24	A'			1299	1296	7.102	0.082	bCCH(53),CC(30),bring1(10),bring2(7)
25	A'		1273	1272	1269	34.335	7.318	bCCH(42),CC(37),bring2(9)

26	A'	1224		1225	1221	7.629	4.372	bmopr(28),CC(28),bCCH(26),bmipr(11)
27	A'			1210	1206	85.296	11.934	bCCH(36),CO(21),CC(15),bmopr(14),bmipr(6)
28	A'		1197	1196	1192	0.323	3.393	bCCH(60),CC(24),bmopr(5)
29	A'			1192	1188	2.546	2.646	bmipr(52),bmopr(24),bmopb(13),bmipb(9)
30	A"	1190		1189	1187	0.745	5.599	gCH(61),gCO(35)
31	A'		1163	1165	1161	24.071	2.510	bCCH(42),CC(32),bring1(11),CO(8),bring2(7)
32	A'			1084	1081	44.747	0.425	CO(59),CC(18),bCCH(12)
33	A'	1049		1050	1047	3.907	19.078	CC(79),bCCH(20)
34	A"		990	992	988	0.039	0.067	gCH(87),tring2(12)
35	A'	971		972	969	2.545	5.399	bring1(42),CC(27),bring2(20),CO(7)
36	A"		962	961	957	2.836	0.203	gCH(89),tring2(5)
37	A"			946	944	0.233	0.438	gCH(89),tring1(8)
38	A'	903		902	899	4.072	3.027	bring2(54),CC(19),CO(15),bring1(6)
39	A"		897	896	891	13.045	4.432	gCH(72),tring1(17),tring2(8)
40	A"			869	866	26.557	1.065	gCH(82),tring2(6),tring1(6),gCO(5)
41	A"	824		822	819	30.877	0.096	gCH(83),tring1(6),tring2(6)
42	A'		787	786	783	0.635	40.639	CC(74),bring1(11),bring2(10)
43	A"			772	769	3.747	6.053	tring2(44),tring1(37),gCH(15)
44	A"	763		765	762	17.532	5.267	gCH(85),gCO(6)
45	A'		720	719	714	8.286	1.076	bring1(38),CC(22),CO(18),bring2(10),bCOC(5)
46	A"			656	654	0.000	0.107	tring1(36),gCO(27),tring2(22),gCH(15)
47	A"	636		635	632	5.155	0.685	tring2(60),tring1(29)
48	A'		563	562	558	8.785	3.356	bCOC(28),bring2(23),bCO(22),bring1(14),CC(5)
49	A"			545	541	0.227	0.575	tring2(46),tring1(17),gCO(17),gCH(17)
50	A'	531		529	525	0.767	10.452	bring1(35),bring2(34),CC(19),bCOC(9)
51	A"			489	487	9.371	0.075	tring1(30),tbutte(28),tring2(25),gCH(11),gCO(6)
52	A"		418	419	416	0.232	2.530	tring1(41),tring2(36),gCH(17)
53	A'	403		405	401	0.146	4.168	bring1(63),CC(13),bCO(11),CO(6)
54	A'			346	341	1.093	7.753	bCOC(45),bring2(22),CC(19),bring1(8)
55	A"		316	315	312	1.489	0.357	tring2(33),tring1(21),tCH3(17),gCH(16),gCO(6)
56	A"			246	243	0.046	0.144	tCH3(64),tring2(17),tring1(7)
57	A'		214	216	212	1.923	0.277	bCO(48),bCOC(21),bring2(13),CC(12)
58	A"			186	184	0.401	0.022	tring1(34),tring2(29),tbutte(12),gCH(11),tCH3(9)
59	A"		133	135	132	1.007	2.673	tring1(32),tCOm(27),tring2(16),gCH(11),tbutte(7)
60	A"			68	65	3.707	1.332	tCOm(59),tCH3(27),tring1(5)

Abbreviations used: b, bending; g, wagging; t, torsion; s, strong; vs, very strong; w, weak; vw, very weak;

[a] Relative absorption intensities normalized with highest peak absorption

[b] Relative Raman intensities calculated by Eq 1 and normalized to 100.

[c] For the notations used see Table 4.

Table 6. Second order perturbation theory analysis of Fock Matrix in NBO basis corresponding to the intramolecular bonds of 2MN

Donor(I)	Types of Bond	Occupancy	Acceptor(J)	Type of Bond	Occupancy	E(2) Kcal/Mol	E(i)-E(j) a.u.	F(i,j)
C1-C2	σ	1.97824	C1-C10	σ*	0.02216	2.99	1.31	0.056
			C1-H13	σ*	0.01378	1.20	1.12	0.033
			C2-C3	σ*	0.02961	3.84	1.29	0.063
			C3-H14	σ*	0.01456	2.36	1.12	0.046
			C9-C10	σ*	0.02344	3.20	1.31	0.058
			O11-C12	σ*	0.00622	1.27	1.01	0.032
C1-C2	π	1.71628	C3-C4	π*	0.27564	18.91	0.29	0.067
			C5-C10	π*	0.48989	18.19	0.31	0.071
C1-C10	σ	1.96778	C1-C2	σ*	0.02464	2.75	1.28	0.053
			C1-H13	σ*	0.01378	0.99	1.11	0.030
			C2-O11	σ*	0.03205	4.53	1.02	0.061
			C5-C6	σ*	0.02371	2.98	1.29	0.056
			C5-C10	σ*	0.03819	4.64	1.30	0.070
			C8-C9	σ*	0.01444	1.99	1.29	0.045
			C9-C10	σ*	0.02344	3.99	1.29	0.064
C1-H13	σ	1.97820	C2-O11	σ*	0.03205	4.53	1.02	0.061
			C5-C6	σ*	0.02371	2.98	1.29	0.056
			C5-C10	σ*	0.03819	4.64	1.30	0.070
			C8-C9	σ*	0.01444	1.99	1.29	0.045
C2-C3	σ	1.97890	C1-C2	σ*	0.02464	17.69	0.28	0.065
			C3-C4	σ*	0.01365	18.76	0.28	0.068
			C6-C7	σ*	0.01449	18.07	0.28	0.067
			C8-C9	σ*	0.01444	17.34	0.28	0.066
C2-O11	σ	1.98746	C1-C2	σ*	0.02464	0.52	1.41	0.024
			C1-C10	σ*	0.02216	1.45	1.43	0.041

			C3-O11	σ*	0.01957	1.49	1.42	0.041
			C12-H20	σ*	0.01091	1.66	1.24	0.040
C3-C4	σ	1.97575	C2-C3	σ*	0.02961	3.05	1.28	0.056
			C2-O11	σ*	0.03205	4.23	1.02	0.059
			C3-H14	σ*	0.01456	1.26	1.11	0.033
			C4-C5	σ*	0.02342	3.04	1.30	0.056
C3-C4	π	1.73824	C5-C10	π*	0.48989	17.49	0.30	0.069
			C1-C2	π*	0.30752	20.59	0.29	0.070
C3-H14	σ	1.97695	C6-C7	σ*	0.01449	0.81	1.11	0.027
			C7-H17	σ*	0.01368	1.00	1.12	0.030
C4-C5	σ	1.97181	C8-H18	σ*	0.01358	0.99	1.12	0.030
			C9-H19	σ*	0.01379	2.53	1.11	0.047
C4-H15	σ	1.98146	C2-C3	σ*	0.02961	3.67	1.09	0.057
			C3-C4	σ*	0.01365	0.86	1.11	0.028
			C4-C5	σ*	0.02342	0.93	1.11	0.029
			C5-C10	σ*	0.03819	4.66	1.12	0.065
C5-C6	σ	1.97158	C1-C10	σ*	0.02216	2.90	1.30	0.055
			C3-C4	σ*	0.01365	2.02	1.29	0.046
			C4-C5	σ*	0.02342	4.15	1.29	0.065
			C5-C10	σ*	0.03819	4.72	1.30	0.070
C5-C10	σ	1.95849	C1-C10	σ*	0.02216	4.12	1.29	0.066
			C1-H13	σ*	0.01378	2.21	1.10	0.044
			C4-C5	σ*	0.02342	4.17	1.29	0.066
C5-C10	π	1.52228	C1-C2	π*	0.30752	17.69	0.28	0.065
			C3-C4	π*	0.73824	18.76	0.28	0.068
			C6-C7	π*	0.72416	18.07	0.28	0.067
			C8-C9	π*	0.27232	17.34	0.28	0.066
C6-C7	σ	1.98001	C5-C6	σ*	0.02371	3.07	1.30	0.056
			C6-H16	σ*	0.98163	1.08	1.11	0.031
			C7-C8	σ*	0.01604	2.79	1.29	0.054
C6-C7	π	1.72416	C5-C10	π*	0.48989	17.49	0.30	0.069
			C8-C9	π*	0.27232	19.99	0.29	0.068
C6-H16	σ	1.98157	C5-C6	σ*	0.02371	0.73	1.07	0.025
			C5-C10	σ*	0.03819	4.25	1.06	0.060
			C6-C7	σ*	0.01449	1.08	1.13	0.031
			C7-C8	σ*	0.01604	3.85	1.07	0.057
C7-C8	σ	1.97981	C6-C7	σ*	0.01449	2.58	1.29	0.052
			C6-H16	σ*	0.01386	2.70	1.14	0.050
			C7-H17	σ*	0.01368	0.94	1.15	0.029
C7-H17	σ	1.98273	C5-C6	σ*	0.02371	4.11	1.07	0.059
			C6-C7	σ*	0.01449	1.08	1.13	0.031
			C7-C8	σ*	0.01604	0.56	1.07	0.022
C8-C9	σ	1.98143	C1-C10	σ*	0.02216	3.00	1.27	0.055
			C7-C8	σ*	0.01604	2.46	1.25	0.050
C8-C9	π	1.75418	C5-C10	π*	0.48989	16.04	0.29	0.065
			C6-C7	π*	0.27392	16.67	0.29	0.063
C8-H18	σ	1.98253	C6-C7	σ*	0.01449	3.20	1.13	0.054
			C7-C8	σ*	0.01604	0.53	1.07	0.021
C9-C10	σ	1.97130	C1-C2	σ*	0.02464	2.08	1.28	0.046
			C1-C10	σ*	0.02216	4.22	1.30	0.066
			C4-C5	σ*	0.02342	2.97	1.29	0.055
			C5-C10	σ*	0.03819	4.72	1.30	0.070
C9-H19	σ	1.98155	C5-C10	σ*	0.03819	4.69	1.12	0.065
			C7-C8	σ*	0.01604	3.58	1.10	0.056
			C8-C9	σ*	0.01444	0.82	1.10	0.027
			C9-C10	σ*	0.02344	0.91	1.11	0.028
O11-C12	σ	1.98507	C1-C2	σ*	0.02464	1.77	1.40	0.045
O11-C12	π	1.98456	C1-C2	π*	0.30752	2.19	0.84	0.042
C12-H20	σ	1.99096	C2-O11	σ*	0.03205	2.96	0.84	0.045
C12-H22	σ	1.99749	C2-O11	σ*	0.03205	0.53	0.83	0.019
O11	LP(1)	1.95732	C1-C2	π*	0.30752	1.33	0.57	0.026
			C2-C3	σ*	0.02961	5.17	1.12	0.068
			C12-H20	σ*	0.01091	1.23	0.95	0.031
			C12-H21	σ*	0.02253	3.22	0.93	0.049
	LP(2)	1.90753	C1-C2	σ*	0.02464	4.18	0.92	0.056
			C1-C2	π*	0.30752	9.51	0.37	0.056
			C2-C3	σ*	0.02961	1.81	0.91	0.037
			C12-H21	σ*	0.02253	3.16	0.73	0.044
			C12-H22	σ*	0.02179	7.13	0.74	0.066

Delocalization of electron density between occupied Lewis-type (bond or lone pair) NBO orbitals and formally unoccupied (antibond or Rydgberg) non Lewis NBO orbitals correspond to a stabilization donor–acceptor interaction. NBO analysis has been performed for 2MN molecule at the DFT/B3LYP/6-311+G** level in order to elucidate the intramolecular, rehybridization and delocalization of electron density within the molecule.

The intramolecular interaction are formed by the orbital overlap between σ(c-c), σ*(c-c), π(c-c), π*(c-c) bond orbital which intermolecular charge transfer(ICT) causing stabilization of the system. These interactions are observed as increase in Electron Density (ED) in C-C antibonding orbitals that weakens the respective bonds. These intermolecular charge transfer (σ-σ*, π- π*) can induce large non-linearity of the molecule. The strong intramolecular hyper conjugative interaction of the σ electron of (C3–C4) distribute to σ*(C2–C3), C2–O11, C3–H14 and C4–C5 of the ring. On the other hand, side the π(C3–C4) in the ring conjugate to the anti-bonding orbital of π*(C5–C10) and π*(C1–C2) which leads to strong delocalization of 17.4 and 20.5 kJ/mol. The π(C6–C7) bond is interacting with π*(C5–C10) and π*(C8–C9) with the energies 17.4 and 19.9 kcal/mol for 2MN. The σ(C2–C3) bond is contributing energy by 17.6 kcal/mol with σ*(C1–C2). In reverse trend, the σ*(C1–C2) bond is contributing energy by 3.84 kcal/mol with σ*(C2–C3). The most important interactions in the title molecule having lonepair O11 with that of antibonding π*(C1-C2) results to the stabilization of 9.51 kj/mol as shown in the Table 6.

First-order hyperpolarizability calculations

In the presence of an applied electric field, first-order hyperpolarizability is a third rank tensor that can be described by a 3×3×3 matrix. The components of the 3D matrix can be reduced to 10 components because of the Kleinman symmetry [31]. The matrix can be given in the lower tetrahedral format. It is obvious that the lower part of the 3×3×3 matrix is a tetrahedral. The calculation of NLO properties with high accuracy is challenging and requires consideration of many different issues.Computational techniques are becoming valuable in designing, modeling and screening novel NLO materials. The calculated value of hyperpolarizability for the 2MN is 84.226×10^{-30} esu, which is greater than that of urea (0.1947×10^{-30} esu). The calculated values of dipole moment and hyperpolarizability values are tabulated in Table 7. The β_{zyy} direction shows biggest value of hyperpolarizability which insists that the delocalization of electron cloud is more on that direction than other directions.

The static polarizability value [32-33] is proportional to the optical intensity and inversely proportional to the cube of transition energy. With this concept, larger oscillator strength (f_n) and $\Delta\mu_{gn}$ with lower transition energy (E_{gn}) is favourable to obtain large first static polarizability values.Electronic excitation energies, oscillator strength and nature of the respective excited states were calculated by the closed-shell singlet calculation method and are summarized in Table 8. Fig. 4 shows the highest occupied molecule orbital (HOMO) and lowest unoccupied molecule orbital (LUMO) of 2MN.Orbital involved in the electronic transition for (a) HOMO−0 (b) LUMO+0 (c) HOMO-1 (d) LUMO+1 (e) HOMO-2 (f) LUMO+2 is represented in Fig 5. The NLO responses can be understood by examining the energetic of frontier molecular orbitals. There is an inverse relationship between hyperpolarizability and HOMO–LUMO.

HOMO energy = -0.032 a.u
LUMO energy = 0.003 a.u
HOMO–LUMO energy gap = 0.035 a.u

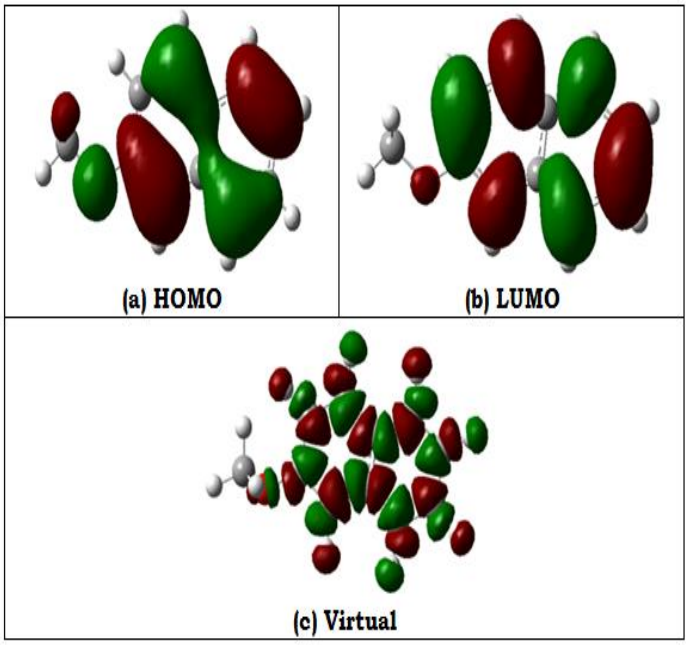

Fig 4. Representation of the orbital involved in the electronic transition for (a) HOMO (b) LUMO (c) Virtual

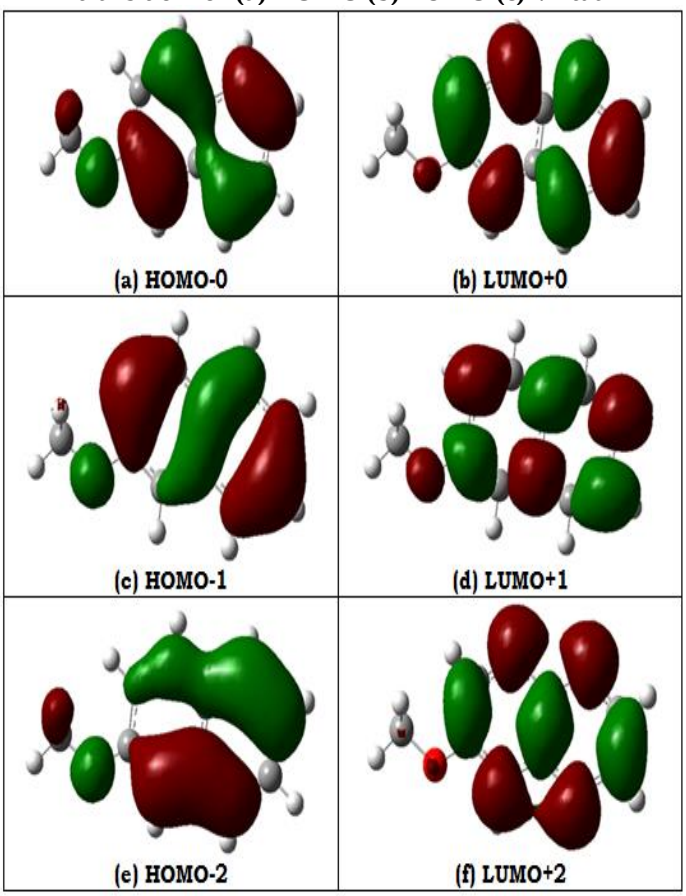

Fig 5. Representation of the orbital involved in the electronic transition for (a) HOMO−0 (b) LUMO+0 (c) HOMO-1 (d) LUMO+1 (e) HOMO-2 (f) LUMO+2

Table 7. The dipole moment (μ) and first-order hyperpolarizibility (β) of 2MN derived from DFT calculations

β_{xxx}	**46.622**
β_{xxy}	-375.43
β_{xyy}	-12.59
β_{yyy}	-32.608
β_{zxx}	-20.063
β_{xyz}	630.19
β_{zyy}	761.01
β_{xzz}	31.304
β_{yzz}	-14.294
β_{zzz}	-364.79
β_{total}	84.226
μ_x	0.17136263
μ_y	0.26379123
μ_z	0.01354279
μ	0.66984823

Dipole moment (μ) in Debye, hyperpolarizibility $\beta(-2\omega;\omega,\omega)$ 10^{-30}esu.

Table 8. Computed absorption wavelength (λ_{ng}) , energy (E_{ng}), oscillator strength (f_n) and its major contribution

n	λ_{ng}	E_{ng}	f_n	Major contribution
1	242.9	5.11	0.1355	H-0->L+0(+82%)
2	229.8	5.40	0.0012	H-1->L+0(+49%), H-0->L+1(+47%)
3	174.7	7.10	0.0014	H-0->L+2(+62%), H-2->L+0(+30%)

(Assignment; H=HOMO,L=LUMO,L+1=LUMO+1,etc.)

Conclusions

In this work, density functional theory calculations were calculated on the structure and vibrational spectrum of 2MN. Vibrational frequencies, Infrared intensities and Raman activities calculated by B3LYP/6-311+G** method agree very well with experimental results. On the basis of agreement between the calculated and observed results, an assignment of all the fundamental vibrational modes of 2MN was examined. Therefore, the assignments made at higher level of theory with higher basis set with only reasonable deviations from the experimental values, seem to be correct. This study demonstrates that scaled B3LYP/6-311+G** calculations are powerful approach for understanding the vibrational spectra of medium sized organic compounds. Comparison of the IR intensities and Raman activities calculated by B3LYP/6-311+G** level with experimental values exposes the variation of IR intensities and Raman activities. The force field determined was used to calculate the vibrational potential energy distribution among the normal coordinate. The stability and intramolecular interactions have been interpreted by NBO analysis and the transactions give stabilization to the structure have been identified by second order perturbation energy calculations. The first-order hyperpolarizability (β_{total}) of 2MN was calculated and found to be 84.226×10^{-30} esu, which is greater than that of urea (0.1947×10^{-30} esu). Electronic excitation energies, oscillator strength and nature of the respective excited states were calculated by the closed-shell singlet calculation method. The NLO responses can be understood by examining the energetic of frontier molecular orbitals.

References

1. V. Krishnakumar, R. Mathammal, S. Muthunatesan, Spectrochimica Acta. 70 A (2008) 201.
2. M. Arivazhagan V. Krishnakumar. John Xavier, G . Ilango V . Balachandran, Spectrochim Acta A (Article in press)
3. D. Sajan, J. Binoy, B. Pradeep, K. Venkatakrishnan, V.B. Kartha, I.H. Joe, V.S. Jayakumar, Spectrochim. Acta. 60A (2004) 173.
4. J.P. Abraham, I.H. Joe, V. George, O.F. Nielson, V.S. Jayakumar, Spectrochim. Acta. 59 A (2003) 193.
5. M. J. Frisch, G. W. Trucks, H. B. Schlegel, G. E. Scuseria, M. A. Robb, J. R. Cheeseman, G. Scalmani, V. Barone, B. Mennucci, G. A. Petersson, H. Nakatsuji, M. Caricato, X. Li, H. P. Hratchian, A. F. Izmaylov, J. Bloino, G. Zheng, J. L. Sonnenberg, M. Hada, M. Ehara, K. Toyota, R. Fukuda, J. Hasegawa, M. Ishida, T. Nakajima, Y. Honda, O. Kitao, H. Nakai, T. Vreven, J. A. Montgomery, Jr., J. E. Peralta, F. Ogliaro, M. Bearpark, J. J. Heyd, E. Brothers, K. N. Kudin, V. N. Staroverov, R. Kobayashi, J. Normand, K. Raghavachari, A. Rendell, J. C. Burant, S. S. Iyengar, J. Tomasi, M. Cossi, N. Rega, J. M. Millam, M. Klene, J. E. Knox, J. B. Cross, V. Bakken, C. Adamo, J. Jaramillo, R. Gomperts, R. E. Stratmann, O. Yazyev, A. J. Austin, R. Cammi, C. Pomelli, J. W. Ochterski, R. L. Martin, K. Morokuma, V. G. Zakrzewski, G. A. Voth, P. Salvador, J. J. Dannenberg, S. Dapprich, A. D. Daniels, O. Farkas, J. B. Foresman, J. V. Ortiz, J. Cioslowski, and D. J. Fox, Gaussian, Inc., Wallingford CT, 2009.
6. J.Binoy, J.P.Abraham, I.H.Joe, V.S.Jayakumar, J.Aubard, O.F.Nielson J.Raman Spectrosc. 36 (2005) 63.
7. P. Hohenberg, W. Kohn, Phys. Rev. 136 (1964) B864.
8. A.D. Becke, J. Chem. Phys., 98 (1993) 5648.
9. C. Lee, W. Yang, R.G. Parr, Phys. Rev., B37 (1988) 785.
10. A. Frisch, A.B. Nielson, A.J. Holder, GAUSSVIEW User Manual, Gaussian Inc., Pittsburgh, PA, 2000.
11. G. Keresztury, S. Holly, J. Varga, G. Besenyei, A.Y. Wang, J.R. Durig, Spectrochim. Acta 49A (1993) 2007.
12. G. Keresztury, in: J.M. Chalmers, P.R. Griffiths (Eds.), Raman Spectroscopy: Theory in Handbook of Vibrational Spectroscopy, vol.1, John Wiley & Sons Ltd., 2002.
13. G. Foragarasi, P. Pulay, in: J.R. Durig (Ed.), Vibrational Spectra and Structure, vol. 14, Elsevier, Amsterdam, 1985, pp. 125–219.

14. P. Pulay, in: H.F. Schaefer III (Ed.), Application of Electronic structure Theory, Modern Theoretical Chemistry, vol. 4, Plenum press, New York, 1997, p. 153.
15. G. Forgarasi, X. Zhou, P.W. Taylor, P. Pulay, J. Am. Chem. Soc. 114 (1992) 8191.
16. G.Varsanyi, Vibrational Spectra of Benzene Derivatives, Academic press, New York, 1969.
17. B.Karthikeyan, Spectrochim Acta. 64A (2006) 1083.
18. T. Bardakc, M. Kumru and S. Guner, Journal of Molecular Structure, 1054 (2013) 76-82.
19. Li Xiao-Hong and Zhang Xian-Zhou, Computational and Theoretical Chemistry, 963 (2011) 34-39.
20. T. Shimanouchi, Y. Kakiuti, I. Gamo, J. Chem. Phys. 25 (1956) 1245.
21. D.L.Vein, N.B.Colthup, W.G.Fateley, J.G.Grasselli, The Handbook of Infrared and Raman Characteristic Frequencies of Organic Molecules, Academic Press, San Diego, 1991.
22. B.Smith, Infrared Spectral Interpretation, A Systematic Approach, CRC Press, Washington, DC, 1999.
23. R.M.Silverstein, F.X.Webster, Spectroscopic Identification of Organic Compounds, sixth ed, John Wiley & Sons Inc., New York, 2003.
24. M. Amalanathan, V.K. Rastogi, I. Hubert Joe, M.A. Palafox and Rashmi Tomar, Spectrochimica Acta Part A: Molecular and Biomolecular Spectroscopy, 78 (2011) 1437-1444.
25. N.B. Colthup, L.H. Paly, S.E.Wiberley, Introduction to Infrared and Raman Spectroscopy, Academic Press, New York, 1990.
26. F.R. Dollish,W.G. Fateley, F.F. Bentely, Characteristic Raman Frequencies on Organic Compounds, Wiley, New York, 1997.
27. M. Szafran, A. Komasa, E.B. Adamska, J. Mol. Struct. (Theochem.) 827 (2007)
28. C. James, A. Amal Raj, R. Rehunathan, I. Hubert Joe, V.S. Jayakumar, J. Raman Spectrosc. 37 (2006) 1381.
29. Liu Jun-na, Chen Zhi-rang, Yuan Shen-fang, J. Zhejiag, University Sci. 6B (2005) 584.
30. S. Sebastian, N. Sundaraganesan, Spectrochim. Acta 75A (2010) 941.
31. D.A. Kleinman, Phys. Rev. 1962;126,1977.
32. K. Wu, C. Liu, C. Mang, Opt. Mater. 29 (2007) 1129–1137.
33. S. Iran, W.M.F. Fabian, Dyes Pigments 70 (2006) 91–96.